Peripheral nervous system plasmalogens regulate Schwann cell differentiation and myelination

Tiago Ferreira da Silva,[1,2] Jessica Eira,[1] André T. Lopes,[1] Ana R. Malheiro,[1] Vera Sousa,[1,2] Adrienne Luoma,[3] Robin L. Avila,[3] Ronald J.A. Wanders,[4] Wilhelm W. Just,[5] Daniel A. Kirschner,[3] Mónica M. Sousa,[1] and Pedro Brites[1]

[1]Nerve Regeneration Group, Instituto de Biologia Molecular e Celular (IBMC), Porto, Portugal.
[2]Instituto de Ciências Biomédicas Abel Salazar (ICBAS), University of Porto, Porto, Portugal.
[3]Biology Department, Boston College, Chestnut Hill Massachusetts, USA. [4]Academic Medical Center, University of Amsterdam, Amsterdam, The Netherlands. [5]Biochemistry Center Heidelberg, University of Heidelberg, Heidelberg, Germany.

Rhizomelic chondrodysplasia punctata (RCDP) is a developmental disorder characterized by hypotonia, cataracts, abnormal ossification, impaired motor development, and intellectual disability. The underlying etiology of RCDP is a deficiency in the biosynthesis of ether phospholipids, of which plasmalogens are the most abundant form in nervous tissue and myelin; however, the role of plasmalogens in the peripheral nervous system is poorly defined. Here, we used mouse models of RCDP and analyzed the consequence of plasmalogen deficiency in peripheral nerves. We determined that plasmalogens are crucial for Schwann cell development and differentiation and that plasmalogen defects impaired radial sorting, myelination, and myelin structure. Plasmalogen insufficiency resulted in defective protein kinase B (AKT) phosphorylation and subsequent signaling, causing overt activation of glycogen synthase kinase 3β (GSK3β) in nerves of mutant mice. Treatment with GSK3β inhibitors, lithium, or 4-benzyl-2-methyl-1,2,4-thiadiazolidine-3,5-dione (TDZD-8) restored Schwann cell defects, effectively bypassing plasmalogen deficiency. Our results demonstrate the requirement of plasmalogens for the correct and timely differentiation of Schwann cells and for the process of myelination. In addition, these studies identify a mechanism by which the lack of a membrane phospholipid causes neuropathology, implicating plasmalogens as regulators of membrane and cell signaling.

Introduction

Plasmalogens, glycerophospholipids with a 1-O-alkenyl ether bond at the *sn*-1 position of the glycerol backbone, represent the most abundant form of ether phospholipids. In vitro studies have highlighted the role of plasmalogens as mediators of the physical properties of membranes, as antioxidants, and as pools of lipid mediators (1). The biosynthesis of ether phospholipids is initiated in peroxisomes by the activity of glyceronephosphate O-acyltransferase (GNPAT) and alkylglyceronephosphate synthase (AGPS) (2). Mutations in *GNPAT*, *AGPS*, or in *PEX7*, which targets AGPS in peroxisomes, lead to extremely reduced levels of plasmalogens and to rhizomelic chondrodysplasia punctata (RCDP) (3–5). RCDP is a peroxisomal disorder characterized by multiple tissue defects, ranging from bone, eye, and heart, to nervous tissue involvement (6, 7). Nevertheless, the pathophysiology behind defective plasmalogens is poorly understood. The phenotype of mouse models for RCDP has supported the etiology of the disease (8). *Pex7*- and *Gnpat*-KO mice, lacking plasmalogens in all tissues, are characterized by a severe phenotype, with early postnatal death and hypotonia in a subset of mice, whereas KO mice surviving past the first 2 weeks display impaired growth, cataracts, and infertility (9, 10). Decreased transcript levels of *Pex7* and *Agps* impair ether phospholipid synthesis in *Pex7* and *Agps* hypomorphic mice, respectively, causing partial decreases in plasmalogen levels. In these mutants, the residual levels of plasmalogens are thought to prevent the hypotonia and early lethality observed in KO mice (11, 12). Nevertheless, bone, lens, and testicular defects in the hypomorphic mice mirror those of KO mice. *Pex7*- and *Gnpat*-KO mice, models of RCDP type 1 and type 2, respectively, share a defect in ether phospholipid biosynthesis, although *Pex7*-KO mice also have defects in fatty acid β- and α-oxidation (9, 13). As in the human RCDP variants, the phenotype and tissue pathology of *Pex7*- and *Gnpat*-KO mice are extremely similar, highlighting that the defect in plasmalogens is the major player in disease presentation and progression.

Plasmalogens are enriched in nervous tissue, especially in white matter, where they localize to the cytoplasmic apposition of myelin (14, 15). Brain imaging of classical RCDP patients indicates impaired myelination, with hypointensity on T1-weighted images and reduced levels of choline, with increased mobile lipids and myo-inositol on MR spectroscopy (6, 16). A plasmalogen deficiency in mice contributes to astrocytosis, microgliosis, and myelin loss in the CNS (13). Impaired peripheral nerve conduction in *Pex7*-KO mice (13) and the description of peripheral neuropathy in a subset of RCDP patients lacking the rhizomelia and ossification defects (17) prompted us to determine the role of plasmalogens and the consequences of their deficiency in the peripheral nervous system (PNS). In the PNS, Schwann cells are the glia responsible for maintaining axonal health and myelination (18). Prior to myelination and concomitant with Schwann cell differentiation, large-caliber axons destined for myelination are seg-

Authorship note: Tiago Ferreira da Silva, Jessica Eira, and André T. Lopes contributed equally to this work.

Conflict of interest: The authors have declared that no conflict of interest exists.

Citation for this article: *J Clin Invest.* 2014;124(6):2560–2570. doi:10.1172/JCI72063.

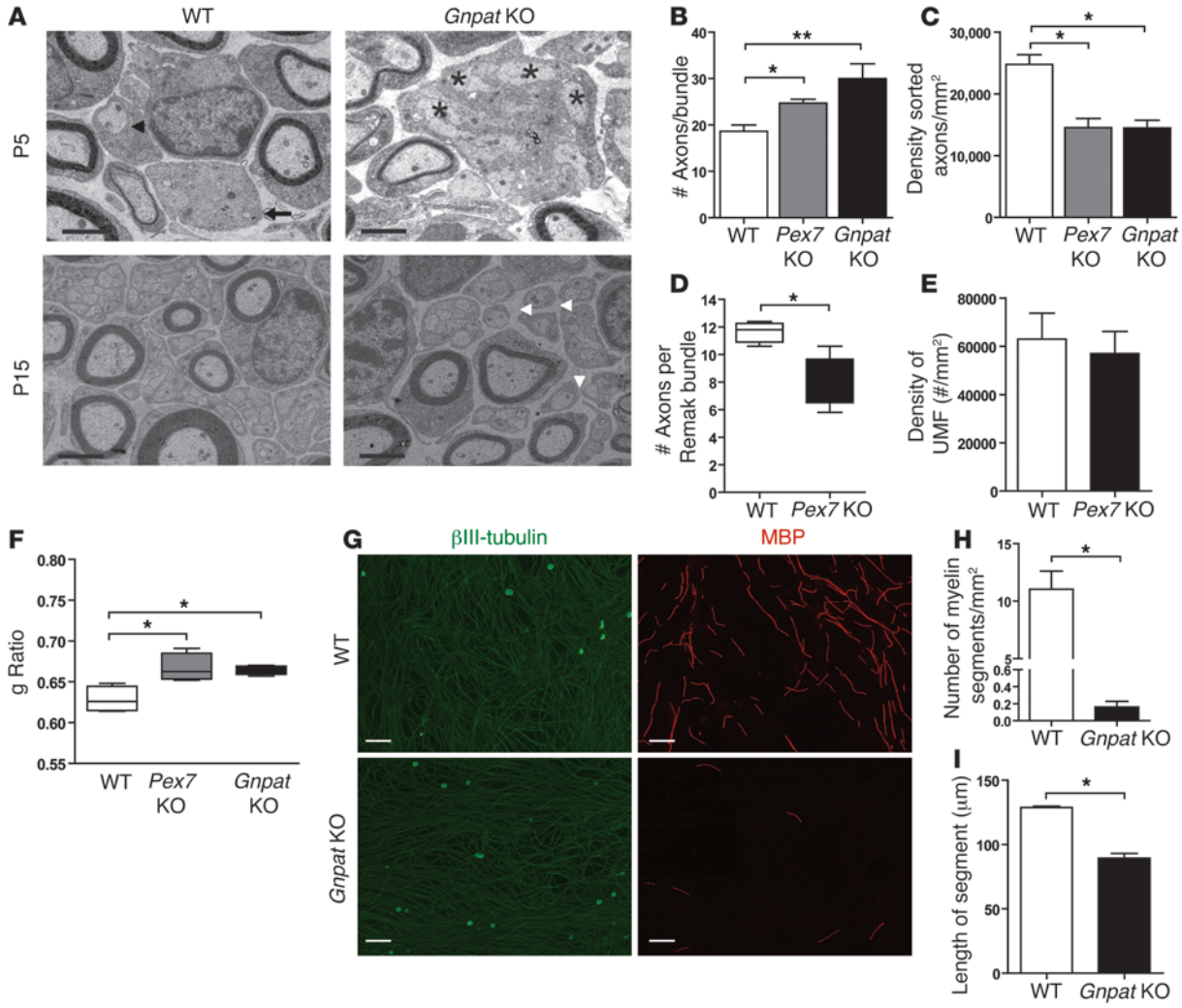

Figure 1

Plasmalogen deficiency causes defects in axonal sorting and myelination. (**A**) Electron microscopic analysis of sciatic nerves from P5 and P15 WT and *Gnpat*-KO mice. Bundles in P5 *Gnpat*-KO nerves contained large axons (asterisks), whereas in WT nerves these axons had been sorted (arrowhead), and the bundles contained very small-caliber axons (arrow). At P15, sciatic nerves from *Gnpat*-KO mice had Remak bundles with only 1 axon (arrowheads). Scale bars: 2 μm. (**B**) Composition of axon bundles in sciatic nerves from P5 WT, *Pex7*-KO, and *Gnpat*-KO mice. **P* = 0.031; ***P* = 0.011. (**C**) Density of sorted axons in sciatic nerves from P5 WT, *Pex7*-KO, and *Gnpat*-KO mice. **P* = 0.003. (**D**) Composition of Remak bundles in nerves from adult WT and *Pex7*-KO mice. **P* = 0.013. (**E**) Density of unmyelinated fibers (UMF) in Remak bundles of nerves from adult WT and *Pex7*-KO mice. (**F**) Quantification of myelin thickness by g ratio in sciatic nerves at P15. Results are graphed as boxes with a line at the mean and whiskers from the minimal to maximal values. **P* = 0.005. (**G**) DRG cocultures of neurons and Schwann cells from WT and *Gnpat*-KO mice stained for neuronal βII-tubulin (green) and for the myelin protein MBP (red). Scale bars: 200 μm. (**H**) Density of myelin segments in DRG cocultures from WT and *Gnpat*-KO mice. **P* = 0.001. (**I**) Length of individual myelin segments in myelinating cocultures. **P* = 0.001.

regated from axon bundles by Schwann cells in a process called radial sorting (19). Differentiated, promyelinating Schwann cells then undergo transcriptional, biochemical, and morphologic changes as they initiate axonal wrapping with a myelin sheath (20, 21). In the PNS, the extent of myelin deposition around individual axons is driven by the axonal expression of neuregulin 1 (NRG1) and by the signaling cascade initiated in Schwann cells expressing the ErbB receptors (22). In the adult PNS, Remak bundles are composed of immature, nonmyelinating Schwann cells that continue to associate with bundles of small-caliber axons that did not undergo radial sorting (23).

Here, we investigated the role of plasmalogens in myelination of the PNS. Our results demonstrate that plasmalogens are crucial for Schwann cell differentiation, as their absence impairs axonal sorting and myelination. Moreover, we found that plasmalogens and myelin basic protein (MBP) are two crucial players that coordinate myelination in the PNS. Mechanistically, we demonstrate that plasmalogens are essential for the correct phosphorylation and activation of protein kinase B (AKT). In mutant sciatic nerves, reduced AKT activity resulted in overt activation of glycogen synthase kinase 3β (GSK3β). Finally, we found that the exogenous inhibition of GSK3β with lithium or

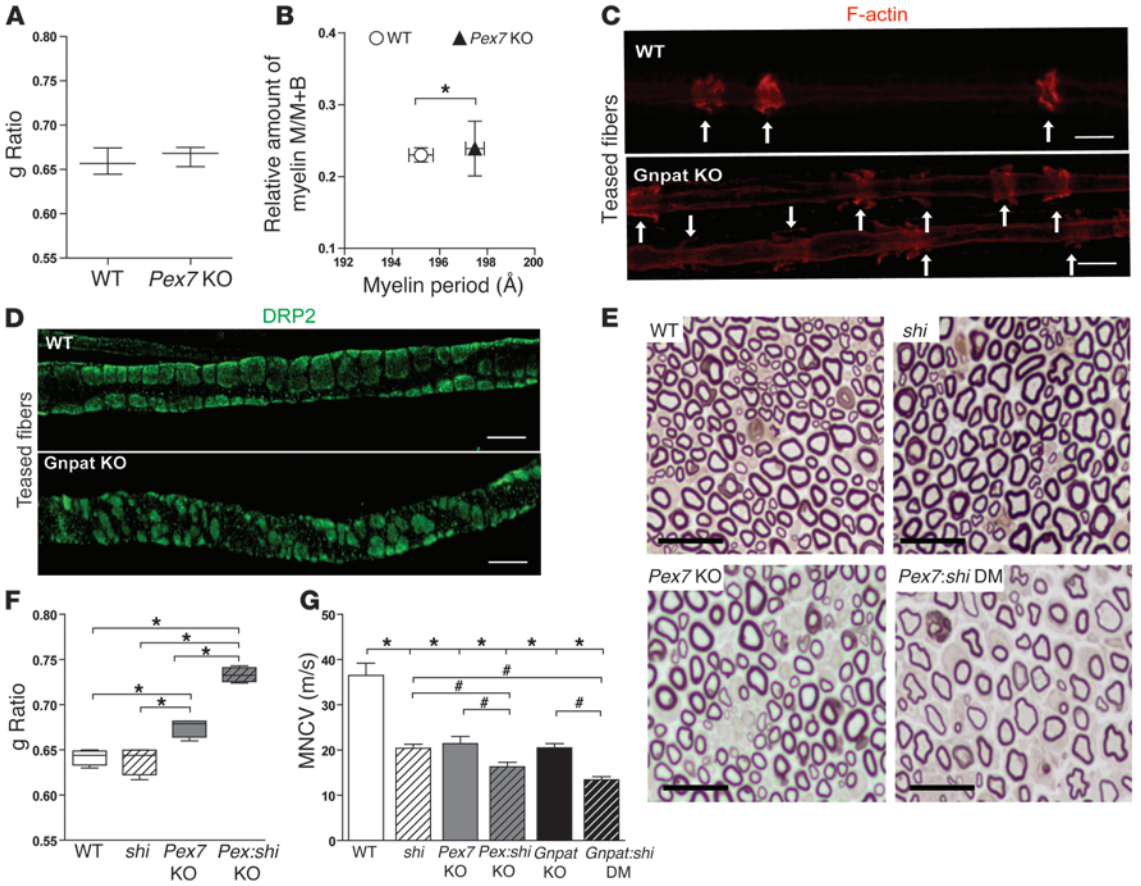

Figure 2

Plasmalogens and MBP coordinate myelination. (**A**) Quantification of myelin thickness by g ratio in sciatic nerves from 3-month-old WT and *Pex7*-KO mice. Results are the mean ± SEM. (**B**) X-ray diffraction analysis of sciatic nerves from WT and *Pex7*-KO mice. Results are graphed as the mean ± SEM. $P = 0.01$. (**C**) Immunofluorescence analysis of teased fibers from adult WT and *Gnpat*-KO nerves stained with F-actin (red). Arrows point to Schmidt-Lanterman incisures. Scale bars: 10 μm. (**D**) Immunofluorescence analysis of sciatic nerve teased fibers stained with an antibody against DRP2 (green) showing abnormal apposition in mutant nerves. Scale bars: 10 μm. (**E**) PPD-stained cross sections of sciatic nerves from P30 mice. Scale bars: 25 μm. (**F**) Quantification of the degree of myelination by g ratio in sciatic nerves from P30 mice. Results are graphed as boxes with a line at the mean and whiskers from the minimal to maximal values. $^{*}P < 0.001$. (**G**) Calculated motor nerve conduction velocities (MNCV) in 3-month-old WT, *shi*, *Pex7*-KO, *Pex7:shi* DM, *Gnpat*-KO, and *Gnpat:shi* DM mice. $^{*}P < 0.0001$; $^{\#}P = 0.001$.

4-benzyl-2-methyl-1,2,4-thiadiazolidine-3,5-dione (TDZD-8) rescued the impairment in Schwann cell differentiation and axonal sorting of plasmalogen-deficient mice. Together, our novel findings reveal the neuropathology behind a deficiency in plasmalogens and elucidate the mechanism by which a membrane phospholipid is essential for Schwann cell differentiation and function, implicating plasmalogens as regulators of membrane and cell signaling.

Results

Plasmalogen deficiency causes defects in radial sorting and myelination. To assess whether *Pex7*- and *Gnpat*-KO mice had defects in PNS development, sciatic nerves from 5- and 15-day-old (P5 and P15, respectively) mice were analyzed by electron microscopy. In nerves from P5 WT mice, we observed axon bundles composed of small-caliber axons (Figure 1A, arrow) and sorted axons (Figure 1A, arrowhead) that displayed a 1:1 relationship with Schwann cells. However, in sciatic nerves from P5 *Gnpat*-KO mice, the bundles contained small- and large-caliber axons (Figure 1A, asterisks). Consistent with a failure in the process of radial sorting, we observed an increased number of axons per bundle (Figure 1B) and a decreased number of sorted, promyelinating fibers (Figure 1C) in nerves from P5 *Pex7*- and *Gnpat*-KO mice. Two main consequences of impaired radial sorting were observed in nerves from *Gnpat*-KO mice. In what seemed to be an attempt by Schwann cells to rescue the impaired radial sorting, we observed an increase in Schwann cells engulfing single, small-caliber axons in nerves from P15 *Gnpat*-KO mice (Figure 1A, white arrowheads). Ultrastructural analysis of sciatic nerves from adult *Pex7*-KO mice revealed a reorganization of Remak bundles, since we observed a reduction in the number of axons in these bundles (Figure 1D), without changes in the density of these unmyelinated fibers (Figure 1E). Additionally, the presence of large-caliber axons in Remak bundles caused Schwann cells to myelinate these structures (Supplemental Figure 1A; supplemental material available online with this article; doi:10.1172/JCI72063DS1). Surprisingly, this abnormal myelination of Remak bundles was not temporary. In sciatic nerves from 1.5-year-old *Gnpat*-KO mice, we continued to observe myelina-

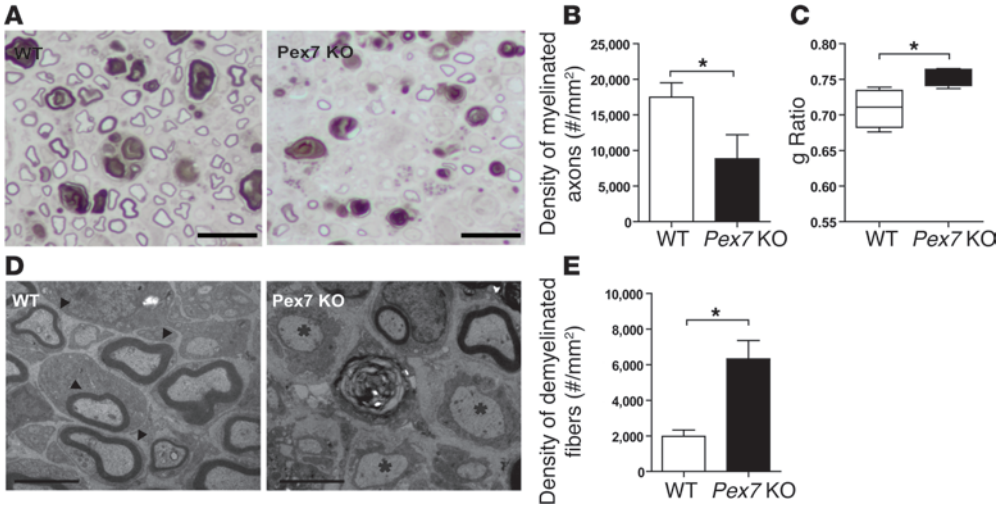

Figure 3

Plasmalogens are important players during remyelination of the PNS. (**A**) PPD-stained cross sections of the distal segment of sciatic nerves 15 days after nerve crush. Scale bars: 10 μm. (**B**) Degree of regeneration as measured by the density of myelinated axons in the distal segment 15 days after sciatic nerve crush. **P* = 0.014. (**C**) Extent of impaired regeneration as measured by g ratio determination. Results are graphed as boxes with a line at the mean and whiskers from the minimal to maximal values. **P* = 0.029. (**D**) Electron microscopic analysis of the distal segment of crushed sciatic nerves from WT and *Pex7*-KO mice. In WT nerves, remyelination of regenerating axons was evident (arrowheads), whereas *Pex7*-KO axons of a similar caliber were devoid of myelin (asterisks). Scale bars: 5 μm. (**E**) Density of axons lacking myelin (demyelinated axons) in the distal segment following sciatic nerve crush. Error bars represent SEM. **P* = 0.012.

tion of Remak bundles that contained a few large-caliber axons (Supplemental Figure 1B).

During postnatal development, from P5 to P20, nerves from *Pex7* and *Gnpat*-KO mice displayed a generalized state of hypomyelination (Supplemental Figure 2). Determination of the g ratio revealed a defect in myelination with decreased myelin thickness in *Pex7*- and *Gnpat*-KO–derived nerves (Figure 1F). In vitro analysis of myelination using cocultures of dorsal root ganglia (DRG) neurons and Schwann cells (Figure 1G) revealed that Schwann cells from *Gnpat*-KO mice produced fewer and smaller myelin segments when compared with those in WT Schwann cells (Figure 1, H and I). These findings demonstrate that deficiency in plasmalogens impairs Schwann cell function, affecting radial sorting and myelination and leading to PNS hypomyelination.

Plasmalogens and MBP coordinate myelination in the PNS. To further address the role of plasmalogens in myelination, we analyzed myelin content in sciatic nerves from adult *Pex7*-KO mice. Surprisingly, we observed normal myelin thickness in mutant nerves (Figure 2A), suggesting a rescue of the defective myelination during postnatal development. However, x-ray diffraction of fixed sciatic nerves showed an increase in myelin period of *Pex7*-KO nerves (Figure 2B), suggesting less compaction or reduced stability of myelin in the absence of plasmalogens. The overall organization of myelinating Schwann cells in teased fiber preparations from *Gnpat*-KO nerves was abnormal, with an increase in noncompact myelin due to the increased number of Schmidt-Lanterman incisures (WT 1.7 ± 0.4 incisures/100 μm, *Gnpat* KO 4.7 ± 1.4 incisures/100 μm; *P* = 0.0028; Figure 2C) and with fragmented and dispersed DRP2-labeled appositions (Figure 2D).

We hypothesized that the achievement of myelination in the absence of plasmalogens could be mediated by the action of other myelin components. Studies of PNS myelin of shiverer (*shi*) mice, which lack MBP, a major constituent of PNS myelin, showed that other myelin components, namely, P0 and P2, are compensatory, allowing *shi* mice to attain normal myelination and compaction (24). To further investigate whether plasmalogens were crucial for myelination, we generated *Pex7:shi* and *Gnpat:shi* double-mutant (DM) mice. Phenotypically, the DMs shared the features of *Pex7*- and *Gnpat*-KO mice and the characteristic shivering caused by MBP deficiency (data not shown). When compared with single mutants and WT mice, nerves from *Pex7:shi* DM mice were characterized by a severe hypomyelination (Figure 2E) without axonal loss (WT 248,704 ± 15,639 axons/mm²; DM 243,884 ± 15,851 axons/mm²; *P* = 0.434). Myelin thickness was reduced in *Pex7*-KO nerves, but the double deficiency of plasmalogens and MBP in *Pex7:shi* DM mice caused a pronounced defect in myelination as judged by the high g ratio values (Figure 2F). At the functional level, the single mutants had defects in nerve conduction, but in DM mice, the combined deficiency of MBP and plasmalogens affected nerve conduction by less than half the normal values (Figure 2G). These findings indicate that in the absence of plasmalogens, the presence of normal amounts of MBP (Supplemental Figure 2B) is sufficient to achieve normal amounts of myelin. Our results highlight the possible coordination between membrane phospholipids and myelin components to attain normal myelination and show that plasmalogen deficiency impairs the organization of myelin and myelinating Schwann cells.

Defects in plasmalogens impair regeneration and preservation of axons and myelin. To further investigate the role of plasmalogens in Schwann cells and myelin, we performed sciatic nerve crush in adult mice. Histological and morphometric analyses performed 15 days after crush in the distal segment of crushed nerves from WT and *Pex7*-KO mice revealed reduced density of remyelinated axons in mutant nerves (Figure 3, A and B). In addition, the extent of remyelination was reduced, showing a higher g ratio in mutant nerves (Figure 3C). Our ultrastructural analysis highlighted that the defect in remyelination was not due to impaired axonal regeneration, as crushed nerves from *Pex7*-KO mice had a 3-fold increase in the density of demyelinated fibers (Figures 3, D and E), i.e., large-caliber axons surrounded by a Schwann cell but lacking myelin sheaths (Figure 3D, asterisks). These results indicate that plasmalogen deficiency primarily affects the ability of Schwann cells to remyelinate regenerating axons.

Analysis of sciatic nerves from aged *Pex7*- and *Gnpat*-KO mice (mean age 17 ± 3.3 months) revealed axonal loss and demyelination (Figure 4A), with decreased numbers of myelinated axons

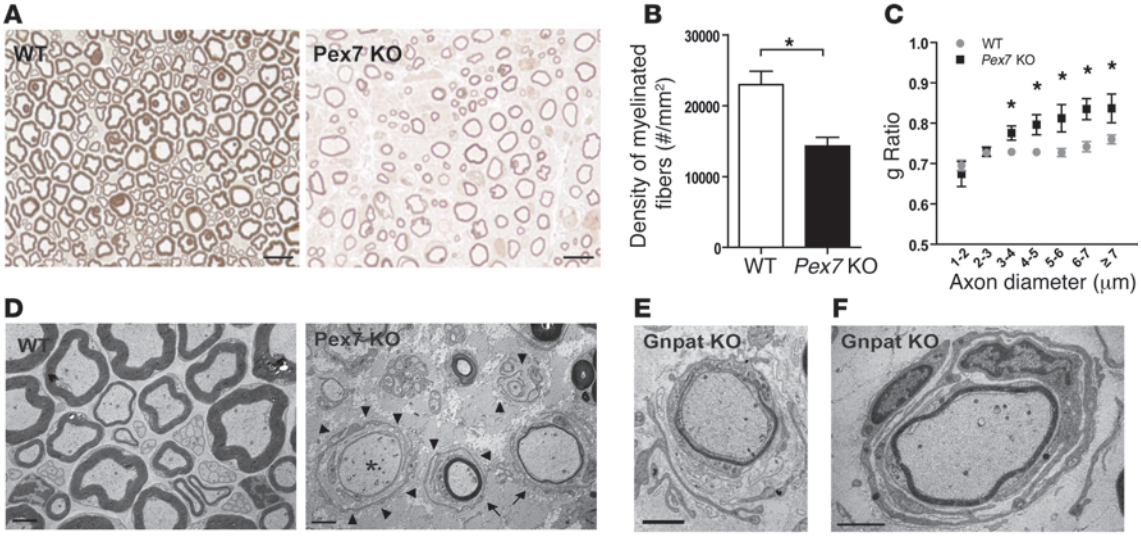

Figure 4

Deficiency in plasmalogens impairs the ability of Schwann cells to sustain myelinated axons. (**A**) PPD-stained cross sections of sciatic nerves from 1.5-year-old WT and *Pex7*-KO mice revealing demyelination and loss of axons in mutant nerves. Scale bars: 10 μm. (**B**) Density of myelinated axons in sciatic nerves from WT and *Pex7*-KO mice. Error bars represent SEM. **P* = 0.012. (**C**) Quantification of the degree of myelination by g ratio in sciatic nerves from 1.5-year-old WT and *Pex7*-KO mice. **P* = 0.026. Error bars represent SEM. (**D**) Electron microscopic analysis of sciatic nerves from representative 1.5-year-old WT and *Pex7*-KO mice showing an axon devoid of myelin (asterisk), severely demyelinated axons (arrows), and the presence of extended Schwann cell processes (arrowheads) throughout the perineurium. Scale bars: 2 μm. (**E**) Schwann cell from an aged *Gnpat*-KO mouse undergoing remyelination of a demyelinated axon. Scale bar: 2 μm. (**F**) Engulfment of a demyelinated axon by 2 Schwann cells, generating concentric deposition of membrane processes, similar to the formation of onion bulbs. Scale bar: 2 μm.

(Figure 4B) and myelin loss in medium- and large-caliber axons (Figure 4C). Ultrastructural analysis showed axons enwrapped by Schwann cells but lacking myelin (Figure 4D, asterisk) and production of redundant basal lamina by mutant Schwann cells (Figure 4D, arrowheads). The endoneurium of plasmalogen-deficient mice was filled with Schwann cell processes, and normal-appearing myelinating Schwann cells also extended processes in an apparent attempt to engulf and enwrap demyelinated and normally myelinated axons (Supplemental Figure 3). In aged *Pex7*- and *Gnpat*-KO mice, attempts at remyelination by mutant Schwann cells were evident by the identification of myelinating images (Figure 4E) that are characteristic of the initial stages of myelination in newborn mice. However, the process of remyelination seemed to be ineffective and abortive, with the formation of onion bulb–like structures (Figure 4F) and axonal loss. Together, our results reveal that during normal development and following nerve regeneration, plasmalogens are crucial for Schwann cells to sort axons, myelinate, and to sustain axons and myelin levels in the PNS.

Plasmalogens regulate AKT activation at the plasma membrane. To elucidate the mechanisms underlying the effects of plasmalogen deficiency in Schwann cells, we analyzed key kinases in sciatic nerves from P15 WT and *Gnpat*-KO mice. Levels of phosphorylated c-Jun N-terminal kinase (JNK), signal transducer and activator of transcription 3 (STAT3), extracellular signal–regulated kinase 1/2 (ERK1/2), and downstream targets of the GTP-binding proteins of the Rho family (namely, N-WASP, myosin light chain, and cofilin) were normal in *Gnpat*-KO nerves (data not shown). However, we observed a 3-fold decrease in AKT phosphorylation (Figure 5A) and in the phosphorylation of two of its targets, GSK3β (Figure 5B) and c-RAF (Figure 5C). The defective phosphorylation of AKT was unrelated to altered levels of phosphorylated PDK1 (Figure 5D) or PTEN (Figure 5E), two upstream regulators of AKT activation. The levels of phosphorylated AKT and GSK3β at Ser9 were reduced in nerve lysates from *Gnpat*-KO mice at P4 (Supplemental Figure 4, A and B), but were normal in lysates from *Gnpat*-KO mice at 3 months of age (Supplemental Figure 4C). During the active period of axonal sorting, we also observed a decrease in the proliferation rate of Schwann cells. Pulse-chase in vivo experiments with BrdU showed reduced BrdU incorporation in sciatic nerves from *Gnpat*-KO mice at P4 (Figure 5F).

Phosphorylation of AKT was also impaired in serum-starved mouse embryonic fibroblasts (MEFs) from *Gnpat*-KO mice after stimulation with 10% FBS (Figure 5G and Supplemental Figure 4D). However, FBS stimulation was able to normally activate ERK1/2 in serum-starved MEFs from KO mice (Figure 5G and Supplemental Figure 4E). We next investigated whether the NRG1/ErbB signaling pathway would also be affected by the plasmalogen deficiency. We measured the levels of AKT phosphorylation in primary Schwann cells from WT and *Gnpat*-KO mice after stimulation with NRG1, the endogenous axonal signal that regulates Schwann cell differentiation and myelination (18). We detected decreased levels of phosphorylation, indicative of impaired AKT activation in Schwann cells from *Gnpat*-KO mice (Figure 5, H and I). The recruitment of AKT to the plasma membrane plays a critical role in its activation by PDK1 and by the mammalian TOR complex 2 (25, 26). Compared with WT MEFs, the plasmalogen deficiency in *Gnpat*-KO MEFs impaired the FBS-induced phosphorylation of AKT at the membrane (Figure 5J and Supplemental Figure 4F), despite normal levels and localization of PDK1 (Supplemental Figure 4G). Failure to activate AKT at the membrane was also evident by the decreased levels of phosphorylated AKT in the cytosolic fraction (Figure 5J). To

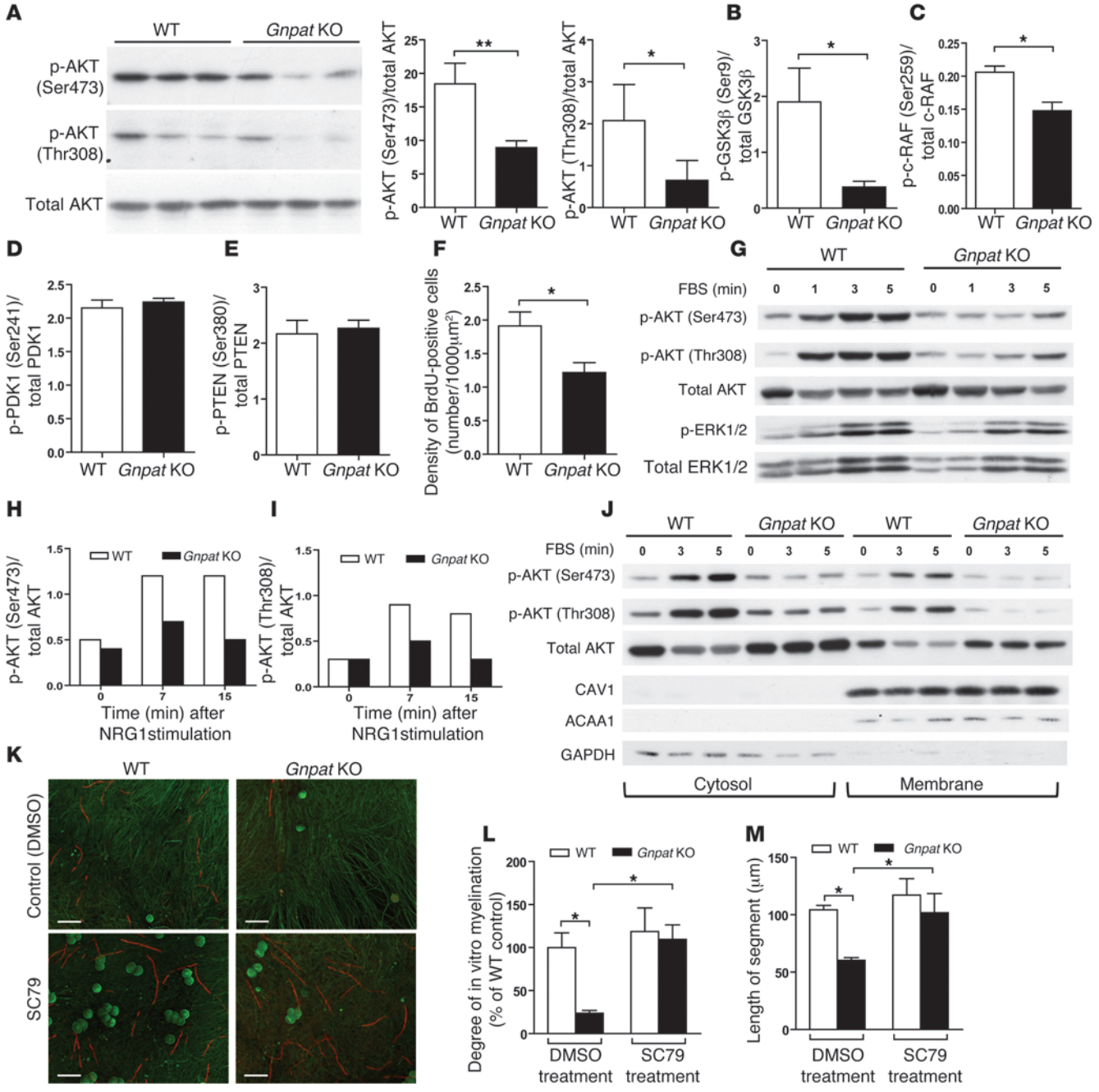

Figure 5

Defects in plasmalogens result in impaired AKT activation and signaling. (**A**) Western blot analysis and quantification of AKT phosphorylation (p-AKT) in sciatic nerve lysates of P15 WT and *Gnpat*-KO mice. **P* = 0.018; ***P* = 0.006. (**B**–**E**) Quantification of phosphorylated forms of GSK3β at Ser9 (**B**), c-RAF at Ser259 (**C**), PDK1 at Ser241 (**D**), and PTEN at Ser380 (**E**) in sciatic nerves from WT and *Gnpat*-KO mice. **P* < 0.02. (**F**) Density of BrdU-positive cells in nerves from P4 WT and *Gnpat*-KO mice. **P* = 0.020. (**G**) Western blot analyses of p-AKT and p-ERK1/2 in serum-starved MEFs from WT and *Gnpat*-KO mice stimulated with 10% FBS. (**H** and **I**) Quantification of p-AKT at Ser473 (**H**) and Thr308 (**I**) in primary WT and *Gnpat*-KO Schwann cells after stimulation with NRG1. (**J**) Western blot analysis of total and p-AKT in cytosolic and membrane fractions of serum-starved MEFs from WT and *Gnpat*-KO mice stimulated with 10% FBS. Western blot analysis of caveolin 1 (CAV1), GAPDH, and peroxisomal thiolase (ACAA1) used to control membrane fractions and cytosolic fractions and to monitor lack of solubilized organelles in cytosolic fractions, respectively. (**K**) DRG cocultures from WT and *Gnpat*-KO mice treated with DMSO (control) or with SC79, stained for neuronal βIII-tubulin (green) and MBP (red). Scale bars: 100 μm. (**L**) Density of myelin segments in DRG cocultures from WT and *Gnpat*-KO mice after DMSO and SC79 treatment. **P* < 0.002. (**M**) Length of individual myelin segments in myelinating cocultures. **P* < 0.01. Error bars represent SEM in all graphs.

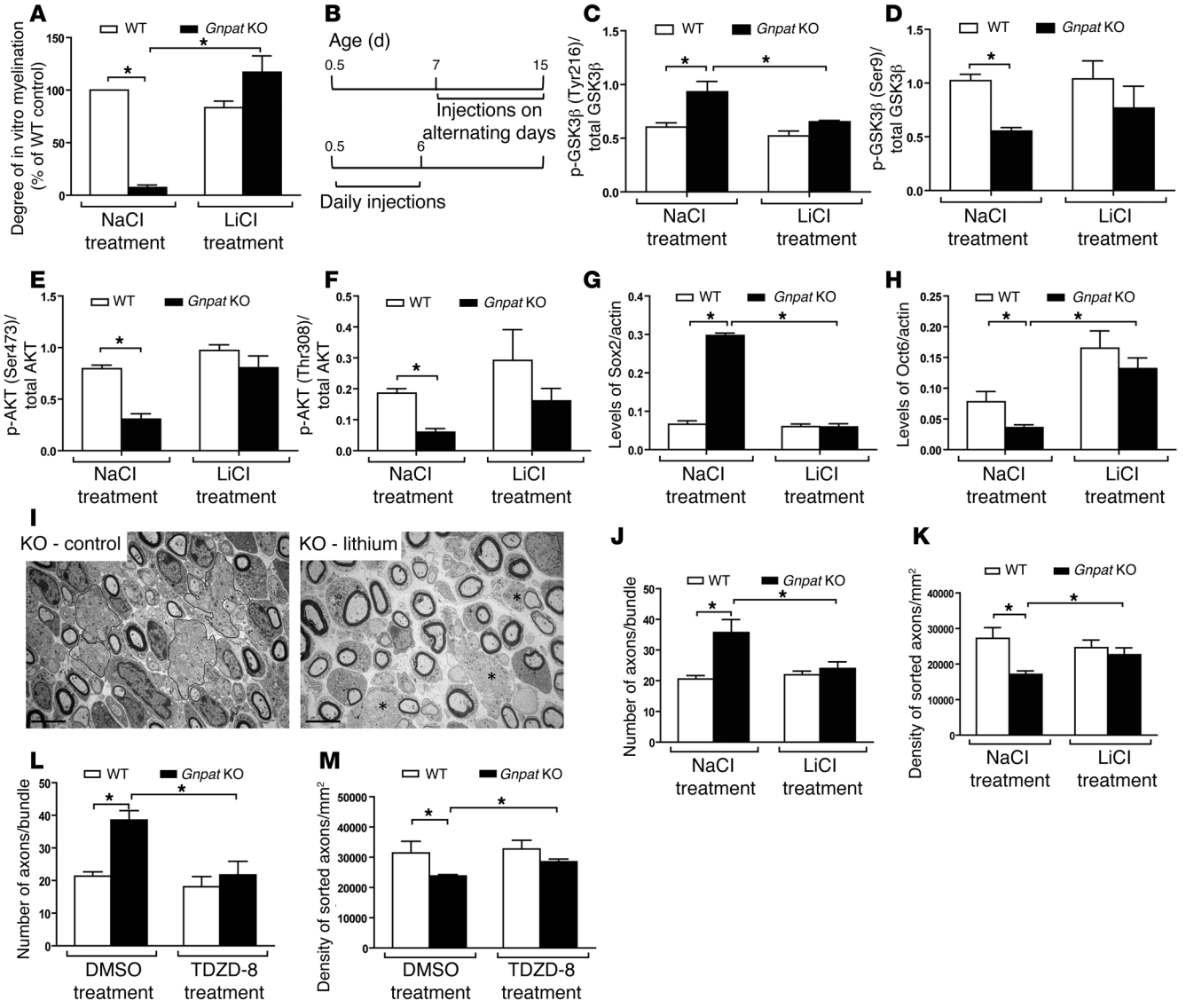

Figure 6

Treatment with GSK3β inhibitors restores Schwann cell differentiation and radial sorting defects. (**A**) In vitro myelination after treatment with NaCl (control) or LiCl. *P = 0.001. (**B**) Strategy for in vivo treatments. For the assessment of LiCl on the phosphorylation of AKT and GSK3β, mice were injected with LiCl on alternating days from P7 to P15 (upper diagram). For the assessment of LiCl on nerve pathology, mice were injected daily with LiCl from P1 to P6 (lower diagram). (**C** and **D**) Quantification of p-GSK3β at Tyr216 (*P = 0.04) (**C**) and Ser9 (*P = 0.017) (**D**) in nerves from P15 mice. (**E** and **F**) Quantification of p-AKT at Ser473 (**E**) and Thr308 (**F**) in nerves from P15 mice. *P = 0.01. (**G** and **H**) Quantification of SOX2 (**G**) and OCT6 (**H**) levels in nerves from P6 WT and *Gnpat*-KO mice. *P = 0.03 (**G**); P = 0.038 (**H**). (**I**) Ultrastructural analysis of sciatic nerves from P6 *Gnpat*-KO mice treated with NaCl and LiCl. Lines and asterisks indicate axon bundles on control and lithium-treated nerves, respectively. Scale bars: 5 μm. (**J**) Number of axons in bundles of sciatic nerves from P6 mice treated with NaCl and LiCl. *P = 0.0013. (**K**) Density of sorted axons (promyelinating stage) in sciatic nerves from P6 mice treated with NaCl and LiCl. *P = 0.0022. (**L**) Number of axons in bundles of sciatic nerves from P4 mice treated with DMSO and TDZD-8. *P < 0.007. (M) Density of sorted axons in sciatic nerves from P4 WT and *Gnpat*-KO mice treated with DMSO and TDZD-8. *P < 0.03.

determine whether the defect in AKT activation plays a critical role in the impaired myelination observed in DRG cocultures, we performed in vitro myelination assays in the presence of SC79. This small compound was shown to allow AKT activation in the cytosol, bypassing the need for AKT to be targeted to the membrane (27). Treatment of DRG cocultures from *Gnpat*-KO mice with SC79 (Figure 5K) increased the number and length of myelin segments (Figure 5, L and M), indicating the rescue in myelination. These results highlight that plasmalogens are important for the correct recruitment and activation of AKT at the membrane and that their absence causes a signaling defect independently of ligand-receptor activation.

Defective differentiation of Schwann cells in plasmalogen-deficient mice is rescued by treatment with GSK3β inhibitors. AKT promotes Schwann cell differentiation and myelination in part through the inhibitory phosphorylation of GSK3β at Ser9 (28). We there-

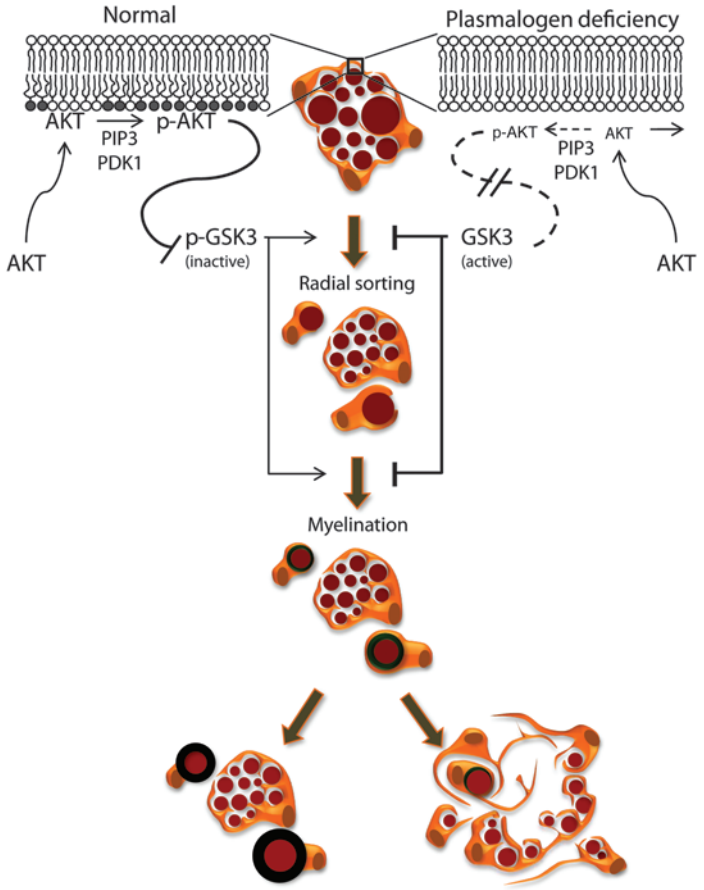

Figure 7
Schematic representation of a proposed model depicting the consequences of plasmalogen deficiency in the PNS. The deficiency in plasmalogens at the plasma membrane of Schwann cells causes reduced phosphorylation of AKT, leading to an overt activation of GSK3β by reducing the inhibitory phosphorylation at Ser9. Active GSK3β inhibits Schwann cell differentiation, impairing axonal sorting and myelination. Lithium administration to inhibit GSK3β is able to rescue Schwann cell differentiation and maturation in the absence of plasmalogens. During aging, lack of plasmalogens causes demyelination and axonal loss, and Schwann cells extend processes in failed attempts to remyelinate existing axons. Plasmalogens are depicted by gray-colored phospholipids; ⚡, impaired signaling; →, induction; ⊤, inhibition.

fore tested whether treatment with LiCl, a GSK3β inhibitor (29), would rescue the Schwann cell defects observed in *Gnpat*-KO mice. The addition of LiCl to the culture medium rescued the myelination defect of DRG mixed cultures from *Gnpat*-KO mice (Figure 6A). Therefore, we treated WT and *Gnpat*-KO mice with LiCl or NaCl in two treatment schemes (Figure 6B). Following LiCl treatment for 1 week from P7, analysis of nerves from *Gnpat*-KO mice revealed decreased phosphorylation of GSK3β at Tyr216 (Figure 6C) and increased phosphorylation of GSK3β at Ser9 (Figure 6D). We found that higher levels of GSK3β phosphorylation at Ser9 were due to increased phosphorylation of AKT (Figure 6, E and F), since lithium dissociates the protein phosphatase 2A–containing (PP2A-containing) complex, decreasing the dephosphorylation of AKT (30).

Lithium treatment during the first 6 days of life induced Schwann cell differentiation in *Gnpat*-KO nerves, as levels of SOX2, a marker of immature Schwann cells, were decreased (Figure 6G), and levels of OCT6, a marker of differentiated Schwann cells, were increased (Figure 6H). Ultrastructural analysis of sciatic nerves from LiCl-treated *Gnpat*-KO nerves showed improved myelination (Figure 6I) and rescue in axonal sorting, with normal numbers of axons in bundles (Figure 6J) and normal density of sorted promyelinating Schwann cells containing a single axon (Figure 6K). Similar results were obtained when newborn WT and *Gnpat*-KO mice were treated for 4 days with TDZD-8, a highly specific inhibitor of GSK3β (31). In sciatic nerves from P4 *Gnpat*-KO mice treated with TDZD-8, we observed a decrease in the number of axons per bundle (Figure 6L) and an increase in the number of sorted axons (Figure 6M). Taken together, our results indicate that plasmalogen deficiency affects Schwann cell differentiation and function, causing defects in axonal sorting, myelination, assembly of myelin, and nerve conduction through the impairment of AKT activation at the plasma membrane and via GSK3β.

Discussion

In this study, we report that a plasmalogen defect in the PNS primarily affects Schwann cells and that plasmalogens are crucial for Schwann cells at two developmental time points. During the early postnatal period, plasmalogens are important for axon-glia interaction and the myelination process. The recognition of axons by Schwann cells or the ability to actively segregate axons destined for myelination is impaired by the deficiency in plasmalogens. The presence of unsorted axons caused abnormal myelination of the Remak bundles and reorganization of these structures. Additionally, impaired myelination, increased regions of noncompact myelin, and defective compartmentalization of Schwann cells in mutant nerves highlight the role of plasmalogens in the correct assembly of myelin and the organization of Schwann cells. Surprisingly, the extent of myelin thickness was normal in adult mutant mice, which led us to hypothesize, that like a deficiency in MBP, which has minimal effects in the PNS despite the complete lack of myelin in the CNS, other myelin components may contribute to achieving normal myelination (24, 32). MBP, known to modulate the apposition of the cytoplasmic leaflets of myelin membranes through electrostatic interactions, is also involved in the partition of myelin into compact and noncompact myelin (33). To further investigate the role of plasmalogens during myelination, we asked whether depleting myelin of plasmalogens and MBP, two major constituents of myelin at the cytoplasmic apposition, would impair myelination. In DM mice, we found a major impairment in myelination and nerve conduction, indicating that plasmalogens are important regulators of myelination. In addition, we found that upon Wallerian degeneration, injury-induced remyelination was also affected by the deficiency in plasmalogens, although axonal regeneration seemed to be unaffected. Failure to maintain myelin levels was also evident in sciatic nerves from aged mutant mice, in which we observed extensive demyelination, axonal loss, and failed attempts to remyelinate the PNS.

Our results highlight that in mice, a deficiency in plasmalogens is sufficient to impair PNS myelination and to cause age-dependent peripheral neuropathy. As such, the evaluation of the PNS

in RCDP type 2 and type 3 patients should be informative. In Refsum's disease, the single defect in α–oxidation of phytanic acid is known to cause peripheral neuropathy (34). Previously, we identified a group of atypical RCDP type 1 patients with mild mutations in PEX7 and a Refsum-like presentation, which included retinitis pigmentosa and nerve hypertrophy (17). In addition to the accumulation of phytanic acid, these patients also had a defect in plasmalogen synthesis. Based on our current findings, we propose that RCDP type 1 patients should also be investigated for defects in nerve conduction and pathology. In these patients, the peripheral neuropathy can be aggravated by the combined defect in plasmalogen synthesis and phytanic acid accumulation.

In the present study, we analyzed the phosphorylation levels of several kinases involved in PNS development to understand how a defect in plasmalogens impairs Schwann cell differentiation and Schwann cell–mediated myelination. The results obtained in nerves of *Gnpat*-KO mice during the active period of myelination in the PNS revealed an impairment of AKT activation. Our observations of impaired activation of the AKT pathway following induction with FBS or NRG1, which was not mediated by defects in upstream regulators, suggested a more direct role of plasmalogens in AKT activation rather than of multiple defects in several ligand-receptor interactions and activations. AKT activation by phosphorylation at the plasma membrane was impaired in plasmalogen-deficient cells. In mutant cells, AKT was found in membrane fractions, but upon FBS stimulation, AKT was not phosphorylated despite the correct localization and phosphorylation of PDK1. The requirement of AKT to associate with raft microdomains for efficient activation and signal transduction, combined with the enrichment of plasmalogens in lipid rafts, suggests that the defect in plasmalogens affects the correct compartmentalization of AKT, and thus its activation by phosphorylation (25, 34). The AKT signaling pathway is important for lens fiber differentiation, chondrocyte differentiation and maturation, adipogenesis, and spermatogenesis (35–38). Based on our results showing that a plasmalogen defect impairs AKT activation in Schwann cells, we hypothesize that in tissues affected by a plasmalogen defect (e.g., lens, cartilage, adipocytes, and testis), impaired AKT signaling modulates the observed pathology, namely, cataracts, impaired ossification, lipodystrophy, and loss of spermatocytes (39).

In sciatic nerves from *Gnpat*-KO mice, we found that impaired AKT activation resulted in dysregulated phosphorylation of GSK3β. GSK3β activity and its role in the regulation of transcription are known to modulate Schwann cell differentiation and myelination (28, 40). Active GSK3β, phosphorylated at Tyr216, is inhibited by AKT phosphorylation at Ser9 (41). In nerves from *Gnpat*-KO mice, we observed increased levels of Tyr216 phosphorylation and decreased levels of Ser9 phosphorylation, which, combined, indicate overtly active GSK3β (41). Lithium, a known inhibitor of GSK3β, can directly inhibit the kinase through Mg^{2+} competition and can indirectly inhibit GSK3β by promoting further inhibition through Ser9 phosphorylation (42, 43). Lithium administration to *Gnpat*-KO mice was able to normalize GSK3β phosphorylation status, induced the stimulation of Schwann cell differentiation, rescued the radial sorting defect, and improved myelination independently of the plasmalogen defect. Similar findings were obtained when *Gnpat*-KO mice were treated with TDZD-8, a highly specific inhibitor of GSK3β. Treatment of plasmalogen-deficient mice with alkyl-glycerol rescues the biochemical defect and pathology in several tissues, but has minimal effects on restoring plasmalogen levels in nervous tissue (39). As such, improving the defective AKT/GSK3β signaling pathway may have clinical potential in combined therapeutic interventions with alkyl-glycerol during the active period of PNS myelination and in mildly affected patients displaying signs of peripheral neuropathy.

In summary, our data reveal the role of plasmalogens in the neuropathic course of two models of RCDP (see proposed model in Figure 7), showing that plasmalogen deficiency severely impairs the ability of Schwann cells to differentiate and mature, thus causing defects in myelination and nerve conduction. Through the identification of the mechanism by which a defect in plasmalogens mediates the pathology, we unraveled that ether phospholipids are crucial for the activation of the AKT pathways and identified a candidate therapeutic intervention that overcomes the plasmalogen deficiency and rescues the signaling pathway and Schwann cell differentiation.

Methods

Mouse strains, procedures, and treatments. WT, *Pex7*, and *Gnpat* mice have been previously described (9, 10). KO and WT littermates of both sexes were obtained from mating of heterozygous mice. Shiverer mice (*shi*; Mbp^{shi}/J) were obtained from The Jackson Laboratory. *Pex7:shi* and *Gnpat:shi* DM mice were obtained from F2 mice after crossing heterozygous *Pex7* or *Gnpat* mice with homozygous *shi* mice.

For nerve crush, 2-month-old WT (n = 4) and *Pex7*-KO (n = 6) mice were anesthetized (i.p. 100 mg/kg ketamine and 1 mg/kg medetomidine), and the exposed right sciatic nerve was injured (15-second crush 2 times) at the level of the notch with a fine hemostat. The contralateral nerve was used as a control. Postsurgical analgesia (1 mg/kg butorphanol s.c.) was performed twice a day for 3 days. Nerve conduction (WT, n = 6; *shi*, n = 4; *Pex7*-KO, n = 3; *Pex7:shi* DM, n = 4; *Gnpat*-KO, n = 5; *Gnpat:shi* DM, n = 3) was determined as previously described (44).

For the BrdU incorporation assay, BrdU in 0.9% NaCl and 7 mM NaOH were injected i.p. at a dosage of 50 mg/kg in WT and *Gnpat*-KO mice (n = 4 for each genotype) 4 and 20 hours before the collection of sciatic nerves.

LiCl or NaCl at a dosage of 50 mg/kg was injected s.c. daily from P0.5 to P6 (control WT, n = 6; *Gnpat*-KO, n = 6; lithium WT, n = 7; *Gnpat*-KO, n = 6) or on alternating days from P7 to P15 (control WT, n = 7; *Gnpat*-KO, n = 7; lithium WT, n = 7; *Gnpat*-KO, n = 7). TDZD-8 (Sigma-Aldrich) at 5 mg/kg or DMSO at 20% (v/v) was injected s.c. daily from P0.5 to P4 (control WT, n= 4; *Gnpat*-KO, n = 4; TDZD-8 WT, n = 5; *Gnpat*-KO, n = 5). Mice were used under standard conditions and had free access to food and water. Experiments and mouse manipulations were performed in compliance with the institutional guidelines and recommendations of the Federation for Laboratory Animal Science Association (FELASA) and were approved by the National Authority for Animal Health (DGAV; Lisbon, Portugal).

Histological and morphological analyses. Sciatic nerves were dissected and fixed by immersion on 4% glutaraldehyde in 0.1 M cacodylate buffer (pH 7.4) for 1 week. After postfixation with 1% OsO_4 in 0.1 M cacodylate buffer (pH 7.4) for 2 hours, nerves were dehydrated and embedded in Epon (Electron Microscopy Sciences). Sections (1-μm-thick) were stained for 10 minutes with 1% p-phenylenediamine (PPD) in absolute methanol, dried, and mounted on a drop of DPX (Merk). The entire area of the nerve was photographed on an Olympus optical microscope equipped with an Olympus DP 25 camera and Cell B software, and images were imported into Photoshop (Adobe). For g ratio analyses, the Photoshop recording measurement tool was used to determine the area of the axon and the entire myelinated fiber (axon plus myelin). Derived diameters were used to calculate the g ratio in 200 to 300 individual fibers per genotype and age (P5 mice: WT, n = 7; *Pex7*-KO, n = 4; *Gnpat*-KO, n = 4; P15 mice: WT, n = 5; *Pex7*-KO, n = 4;

Gnpat-KO, $n = 4$; P30 and P90, $n = 4$ for all genotypes; 1.5-year-old: WT, $n = 6$; *Pex7*-KO, $n = 6$; *Gnpat*-KO, $n = 5$). For the determination of the density of myelinated fibers (MFs), the total number of MFs was divided by the area of the entire cross section of the sciatic nerve.

Ultrathin sections (60-nm) prepared on a Leica ultramicrotome were placed on 200-mesh copper grids (Electron Microscopy Sciences) and were counterstained, first with alcoholic uranyl acetate solution (2% w/v; 10 minutes), then by aqueous uranyl acetate solution (2% w/v; 10 minutes) and lead citrate (4% w/v; 10 minutes). Grids were observed on a JEOL JEM-1400 transmission electron microscope equipped with an Orious Sc1000 digital camera. Ten to 15 nonoverlapping images were obtained and used for all determinations.

Cell culture and in vitro myelination. MEFs were prepared from E12 embryos and cultured in high-glucose DMEM with 10% FBS and antibiotics. Primary Schwann cells were isolated from sciatic nerves of 4-day-old WT and *Gnpat*-KO mice and cultured in high-glucose DMEM with 10% normal horse serum (NHS) and antibiotics. Schwann cells were serum starved for 12 hours before stimulation with 30 ng/ml recombinant human neuregulin 1 β EGF-like domain (R&D Systems). The lysates were prepared after 0, 7, and 15 minutes at 37°C. Serum-starved MEFs were stimulated with 10% FBS for 0, 1, 3, and 5 minutes. The lysates were prepared in PBS containing 0.3% Triton X-100, protease inhibitors (cOmplete, Mini; Roche), and 2 mM orthovanadate.

In vitro myelination was performed as described (45). Mixed cultures of DRG neurons and Schwann cells from WT ($n = 7$) and *Gnpat*-KO ($n = 4$) embryos were maintained in high-glucose MEM with 2 mM L-glutamine, 10% FBS, 50 ng/ml nerve growth factor (NGF) (2.5S; Millipore), and 1% penicillin-streptomycin, and were then plated onto 13-mm-diameter Matrigel-coated coverslides (1:10 in DMEM). After 24 hours at 37°C, cells were cultured for 10 days in neurobasal medium supplemented with 4 g/l glucose, 2 mM L-glutamine, 50 ng/ml NGF, and 1× B27 (Gibco). Myelination was induced at 10 days in vitro (div) by the daily addition of 50 μg/ml ascorbic acid to high-glucose MEM medium supplemented with 2 mM L-glutamine, 10% FBS, and 50 ng/ml NGF. For lithium treatment in myelination assays, medium was supplemented with 3 μM forskolin and 16 mM NaCl (control) or 16 mM LiCl starting at div 7. For treatment with SC79, medium was supplemented with 0.0008% v/v DMSO or with 0.4 μg/ml SC79 (Millipore) in DMSO starting at div 7. In both treatment schemes, cells were fixed and processed for immunofluorescence at 20 div.

Antibodies. The antibodies used were: anti–βIII-tubulin (1:600; 1967-1; Epitomics); anti-MBP (1:250; MAB386; Millipore); anti-DRP2 (1:1,000; ref. 46); anti–Ser473-AKT; anti–Thr308-AKT; anti–pan-AKT; anti–Ser259-c-RAF; anti–Ser9-GSK3β (all at 1:1,000; catalog 9916; Cell Signaling Technology); anti–β-tubulin (1:1,000; catalog 5142; Cell Signaling Technology); anti–caveolin 1 (1:5,000; C13630; BD Transduction Laboratories); anti-ACAA1 (1:1,000; HPA007244; Sigma-Aldrich); anti-GAPDH (1:1,000; catalog 5174; Cell Signaling Technology); and anti-BrdU (1:2,000; Ab6326; Abcam). For immunofluorescence, Alexa Fluor 488– and Alexa Fluor 568–conjugated secondary antibodies were used (1:500; Invitrogen). For detection of BrdU, nerves from P4 WT and *Gnpat*-KO mice were fixed in carnoys and processed for immunofluorescence in paraffin sections pretreated with 2N HCl. For Western blotting, horseradish peroxidase–conjugated secondary antibodies were used (1:5,000; Jackson ImmunoResearch).

Immunofluorescence. In the in vitro myelination assays, fixed and permeabilized cells were incubated for 1 hour at room temperature (RT) with blocking buffer (5% normal donkey serum [NDS] in PBS). Primary antibodies (rabbit anti–βIII-tubulin and rat anti-MBP) were diluted in blocking buffer and incubated for 16 hours at 4°C. After washing with PBS, secondary antibodies were diluted in blocking buffer and incubated for 1 hour at RT. After washing, coverslides were mounted on microscope slides with Vectashield containing DAPI (Vector Labs). Slides were analyzed by epifluorescence on a Zeiss Axio Imager Z1 microscope equipped with an Axiocam MR3.0 camera and Axiovision 4.7 software.

For teased fiber preparations, sciatic nerves from 9-month-old WT and *Gnpat*-KO mice ($n = 3$ for each genotype) were dissected and fixed by immersion with 4% PFA in PBS for 30 minutes. Under a dissection microscope, the perineurium was removed, and small nerve bundles were separated using 30-gauge needles. Nerve bundles were blocked and permeabilized by incubation for 1 hour at RT in blocking buffer containing 0.1% Triton X-100. Bundles were incubated with rhodamine-conjugated phalloidin (1:400; Invitrogen) or with rabbit anti-DRP2 (46) for 16 hours at 4°C. After washing with PBS, bundles were incubated for 2 hours at RT with secondary antibodies. Nerve bundles were then washed in PBS and placed in a drop of Vectashield containing DAPI. Single teased fibers were prepared using 30-gauge needles, sealed, and viewed by confocal microscopy on a Leica TCS SP5 II.

Biochemical analyses. For Western blot analysis, lysates of sciatic nerves were prepared by sonication in lysis buffer, and 25 μg protein was run on 12% SDS-PAGE gels. Blots were developed with ECL (Pierce) and exposed to Hyperfilm (Amersham). Films were scanned on a Molecular Imager GS800, and Quantity One (Bio-Rad) was used for quantifications. The ProteoExtract subcellular proteome extraction kit (Calbiochem) was used to obtain membrane and cytosolic fractions of cultured MEFs from WT and *Gnpat*-KO mice. Three independent experiments were performed.

X-ray diffraction. Sciatic nerves from WT ($n = 6$) and *Pex7*-KO ($n = 7$) mice were fixed by immersion on 2% glutaraldehyde in 0.12 M phosphate buffer (pH 7.4). Diffraction experiments and data analysis were carried out as detailed previously (47). For the determination of the relative amount of myelin by x-ray diffraction, the quotient M/M+B was used, in which the denominator includes the total x-ray scatter coming from the volume of nerve subtended by the x-ray beam (consisting of the multilamellar myelin, M, and background, B), and the numerator is the total intensity coming from the multilamellar myelin (the peak intensities above background), as previously described (47).

Statistics. Results were expressed as the mean ± SEM, and data were analyzed with Prism software (GraphPad Software). To compare 2 groups, nonparametric Mann-Whitney *U* tests were used, and $P < 0.05$ was considered a significant difference. For comparison of more than 2 groups, 1-way ANOVA tests were used, followed by Tukey's multiple comparison tests.

Acknowledgments

We thank Paula Sampaio for microscopy support, Paula Magalhães for genotyping, and Isabel Carvalho, Sofia Lamas, and Fátima Martins for excellent animal care. We are grateful to P. Brophy (University of Edinburgh) for the DRP2 antibody and to M. Baes (K.U. Leuven) for providing the *Gnpat* mouse strain. This work was funded by the Research Foundation of the European Leukodystrophy Association (ELA 2008-009C4, ELA 2010-042C5), by FEDER Funds through the Operational Competitiveness Program – COMPETE, and by national funds through the FCT – Fundação para a Ciência e a Tecnologia under the project FCOMP-01-0124-FEDER-015970 (PTDS/SAU-ORG/112406/2009). P. Brites is an FCT Investigator, and T. Ferreira da Silva was supported by the FCT (SFRH/BD/88160/2012).

Received for publication August 12, 2013, and accepted in revised form February 27, 2014.

Address correspondence to: Pedro Brites, Instituto de Biologia Molecular e Celular, Nerve Regeneration, Rua do Campo Alegre 823, 4150-180, Porto, Portugal. Phone: 351226074900; Fax: 351226099157; E-mail: pedro.brites@ibmc.up.pt.

Adrienne Luoma's present address is: Committee on Immunology, University of Chicago, Chicago, Illinois, USA.

Robin L. Avila's present address is: Department of Neurology, The University of Chicago, Chicago, Illinois, USA.

1. Lessig J, Fuchs B. Plasmalogens in biological systems: their role in oxidative processes in biological membranes, their contribution to pathological processes and aging and plasmalogen analysis. *Curr Med Chem*. 2009;16(16):2021–2041.
2. Wanders RJ, Waterham HR. Biochemistry of mammalian peroxisomes revisited. *Annu Rev Biochem*. 2006;75:295–332.
3. Ofman R, Hettema EH, Hogenhout EM, Caruso U, Muijsers AO, Wanders RJ. Acyl-CoA:dihydroxyacetonephosphate acyltransferase: cloning of the human cDNA and resolution of the molecular basis in rhizomelic chondrodysplasia punctata type 2. *Hum Mol Genet*. 1998;7(5):847–853.
4. de Vet EC, Ijlst L, Oostheim W, Wanders RJ, van den Bosch H. Alkyl-dihydroxyacetonephosphate synthase. Fate in peroxisome biogenesis disorders and identification of the point mutation underlying a single enzyme deficiency. *J Biol Chem*. 1998; 273(17):10296–10301.
5. Motley AM, et al. Mutational spectrum in the PEX7 gene and functional analysis of mutant alleles in 78 patients with rhizomelic chondrodysplasia punctata type 1. *Am J Hum Genet*. 2002;70(3):612–624.
6. Bams-Mengerink AM, et al. MRI of the brain and cervical spinal cord in rhizomelic chondrodysplasia punctata. *Neurology*. 2006;66(6):798–803.
7. White AL, Modaff P, Holland-Morris F, Pauli RM. Natural history of rhizomelic chondrodysplasia punctata. *Am J Med Genet A*. 2003;118A(4):332–342.
8. da Silva TF, Sousa VF, Malheiro AR, Brites P. The importance of ether-phospholipids: A view from the perspective of mouse models. *Biochim Biophys Acta*. 2012;1822(9):1501–1508.
9. Brites P, et al. Impaired neuronal migration and endochondral ossification in Pex7 knockout mice: a model for rhizomelic chondrodysplasia punctata. *Hum Mol Genet*. 2003;12(18):2255–2267.
10. Rodemer C, et al. Inactivation of ether lipid biosynthesis causes male infertility, defects in eye development and optic nerve hypoplasia in mice. *Hum Mol Genet*. 2003;12(15):1881–1895.
11. Braverman N, et al. A Pex7 hypomorphic mouse model for plasmalogen deficiency affecting the lens and skeleton. *Mol Genet Metab*. 2010;99(4):408–416.
12. Liegel R, Chang B, Dubielzig R, Sidjanin DJ. Blind sterile 2 (bs2), a hypomorphic mutation in Agps, results in cataracts and male sterility in mice. *Mol Genet Metab*. 2011;103(1):51–59.
13. Brites P, Mooyer PA, El ML, Waterham HR, Wanders RJ. Plasmalogens participate in very-long-chain fatty acid-induced pathology. *Brain*. 2009; 132(pt 2):482–492.
14. Macala LJ, Yu RK, Ando S. Analysis of brain lipids by high performance thin-layer chromatography and densitometry. *J Lipid Res*. 1983;24(9):1243–1250.
15. Kirschner DA, Ganser AL. Myelin labeled with mercuric chloride. Asymmetric localization of phosphatidylethanolamine plasmalogen. *J Mol Biol*. 1982; 157(4):635–658.
16. Alkan A, Kutlu R, Yakinci C, Sigirci A, Aslan M, Sarac K. Delayed myelination in a rhizomelic chondrodysplasia punctata case: MR spectroscopy findings. *Magn Reson Imaging*. 2003;21(1):77–80.
17. Van den Brink DM, et al. Identification of PEX7 as the second gene involved in Refsum disease. *Am J Hum Genet*. 2003;72(2):471–477.
18. Nave KA, Salzer JL. Axonal regulation of myelination by neuregulin 1. *Curr Opin Neurobiol*. 2006; 16(5):492–500.
19. Jessen KR, Mirsky R. The origin and development of glial cells in peripheral nerves. *Nat Rev Neurosci*. 2005;6(9):671–682.
20. Svaren J, Meijer D. The molecular machinery of myelin gene transcription in Schwann cells. *Glia*. 2008;56(14):1541–1551.
21. Newbern J, Birchmeier C. Nrg1/ErbB signaling networks in Schwann cell development and myelination. *Semin Cell Dev Biol*. 2010;21(9):922–928.
22. Michailov GV, et al. Axonal neuregulin-1 regulates myelin sheath thickness. *Science*. 2004; 304(5671):700–703.
23. Mirsky R, Jessen KR. The biology of non-myelin-forming Schwann cells. *Ann N Y Acad Sci*. 1986; 486:132–146.
24. Kirschner DA, Ganser AL. Compact myelin exists in the absence of basic protein in the shiverer mutant mouse. *Nature*. 1980;283(5743):207–210.
25. Gao X, et al. PI3K/Akt signaling requires spatial compartmentalization in plasma membrane microdomains. *Proc Natl Acad Sci U S A*. 2011; 108(35):14509–14514.
26. Bozulic L, Hemmings BA. PIKKing on PKB: regulation of PKB activity by phosphorylation. *Curr Opin Cell Biol*. 2009;21(2):256–261.
27. Jo H, et al. Small molecule-induced cytosolic activation of protein kinase Akt rescues ischemia-elicited neuronal death. *Proc Natl Acad Sci U S A*. 2012; 109(26):10581–10586.
28. Ogata T, et al. Opposing extracellular signal-regulated kinase and Akt pathways control Schwann cell myelination. *J Neurosci*. 2004;24(30):6724–6732.
29. Freland L, Beaulieu JM. Inhibition of GSK3 by lithium, from single molecules to signaling networks. *Front Mol Neurosci*. 2012;5:14.
30. Mora A, et al. Lithium blocks the PKB and GSK3 dephosphorylation induced by ceramide through protein phosphatase-2A. *Cell Signal*. 2002; 14(6):557–562.
31. Eldar-Finkelman H, Martinez A. GSK-3 inhibitors: preclinical and clinical focus on CNS. *Front Mol Neurosci*. 2011;4:32.
32. Inouye H, Ganser AL, Kirschner DA. Shiverer and normal peripheral myelin compared: basic protein localization, membrane interactions, and lipid composition. *J Neurochem*. 1985;45(6):1911–1922.
33. Aggarwal S, et al. A size barrier limits protein diffusion at the cell surface to generate lipid-rich myelin-membrane sheets. *Dev Cell*. 2011; 21(3):445–456.
34. Pike LJ, Han X, Chung KN, Gross RW. Lipid rafts are enriched in arachidonic acid and plasmenylethanolamine and their composition is independent of caveolin-1 expression: a quantitative electrospray ionization/mass spectrometric analysis. *Biochemistry*. 2002;41(6):2075–2088.
35. Wang Q, Stump R, McAvoy JW, Lovicu FJ. MAPK/ERK1/2 and PI3-kinase signalling pathways are required for vitreous-induced lens fibre cell differentiation. *Exp Eye Res*. 2009;88(2):293–306.
36. Rokutanda S, et al. Akt regulates skeletal development through GSK3, mTOR, and FoxOs. *Dev Biol*. 2009;328(1):78–93.
37. Peng XD, et al. Dwarfism, impaired skin development, skeletal muscle atrophy, delayed bone development, and impeded adipogenesis in mice lacking Akt1 and Akt2. *Genes Dev*. 2003;17(11):1352–1365.
38. Goertz MJ, Wu Z, Gallardo TD, Hamra FK, Castrillon DH. Foxo1 is required in mouse spermatogonial stem cells for their maintenance and the initiation of spermatogenesis. *J Clin Invest*. 2011; 121(9):3456–3466.
39. Brites P, et al. Alkyl-glycerol rescues plasmalogen levels and pathology of ether-phospholipid deficient mice. *PLoS One*. 2011;6(12):e28539.
40. Liang MH, Chuang DM. Differential roles of glycogen synthase kinase-3 isoforms in the regulation of transcriptional activation. *J Biol Chem*. 2006;281(41):30479–30484.
41. Hughes K, Nikolakaki E, Plyte SE, Totty NF, Woodgett JR. Modulation of the glycogen synthase kinase-3 family by tyrosine phosphorylation. *EMBO J*. 1993;12(2):803–808.
42. O'Brien WT, et al. Glycogen synthase kinase-3 is essential for β-arrestin-2 complex formation and lithium-sensitive behaviors in mice. *J Clin Invest*. 2011;121(9):3756–3762.
43. Makoukji J, et al. Lithium enhances remyelination of peripheral nerves. *Proc Natl Acad Sci U S A*. 2012;109(10):3973–3978.
44. Ferdinandusse S, et al. Ataxia with loss of Purkinje cells in a mouse model for Refsum disease. *Proc Natl Acad Sci U S A*. 2008;105(46):17712–17717.
45. Maurel P, et al. Nectin-like proteins mediate axon Schwann cell interactions along the internode and are essential for myelination. *J Cell Biol*. 2007;178(5):861–874.
46. Sherman DL, Wu LM, Grove M, Gillespie CS, Brophy PJ. Drp2 and periaxin form Cajal bands with dystroglycan but have distinct roles in Schwann cell growth. *J Neurosci*. 2012;32(27):9419–9428.
47. Avila RL, et al. Structure and stability of internodal myelin in mouse models of hereditary neuropathy. *J Neuropathol Exp Neurol*. 2005;64(11):976–990.